PHYSICAL REVIEW D **84,** 055014 (2011)

Observations of annual modulation in direct detection of relic particles and light neutralinos

P. Belli,[1] R. Bernabei,[1,2] A. Bottino,[3,4] F. Cappella,[5,6] R. Cerulli,[7] N. Fornengo,[3,4] and S. Scopel[8]
[1]*Istituto Nazionale di Fisica Nucleare, Sezione di Roma Tor Vergata, I-00133 Rome, Italy*
[2]*Dipartimento di Fisica, Università di Roma Tor Vergata, I-00133 Rome, Italy*
[3]*Dipartimento di Fisica Teorica, Università di Torino, I-10125 Torino, Italy*
[4]*Istituto Nazionale di Fisica Nucleare, Sezione di Torino I-10125 Torino, Italy*
[5]*Istituto Nazionale di Fisica Nucleare, Sezione di Roma, I-00185 Rome, Italy*
[6]*Dipartimento di Fisica, Università di Roma La Sapienza, I-00185, Rome, Italy*
[7]*Istituto Nazionale di Fisica Nucleare, Laboratori Nazionali del Gran Sasso, I-67010 Assergi, L'Aquila, Italy*
[8]*Department of Physics, Sogang University, Seoul, Korea, 121-742*
(Received 28 June 2011; published 15 September 2011)

The long-standing model-independent annual modulation effect measured by the DAMA Collaboration, which fulfills all the requirements of a dark matter annual modulation signature, and the new result by the CoGeNT experiment that shows a similar behavior are comparatively examined under the hypothesis of a dark matter candidate particle interacting with the detectors' nuclei by a coherent elastic process. The ensuing physical regions in the plane of the dark matter-particle mass versus the dark matter-particle nucleon cross-section are derived for various galactic halo models and by taking into account the impact of various experimental uncertainties. It is shown that the DAMA and the CoGeNT regions agree well between each other and are well fitted by a supersymmetric model with light neutralinos which satisfies all available experimental constraints, including the most recent results from CMS and ATLAS at the CERN Large Hadron Collider.

DOI: 10.1103/PhysRevD.84.055014 PACS numbers: 95.35.+d, 11.30.Pb, 12.60.Jv, 95.30.Cq

I. INTRODUCTION

An annual-modulation effect, as expected from the relative motion of the Earth with respect to the relic particles responsible for the dark matter (DM) in the galactic halo [1], has been measured by the DAMA Collaboration since long time [2], with an increasing exposure along 13 yrs which, with the second generation DAMA/LIBRA apparatus, has reached the value of 1.17 ton $\times$ year and a confidence level of 8.9σ [3].

A very recent analysis of the data collected by the CoGeNT experiment over a period of 442 days with a very low energy threshold Germanium detector having a fiducial mass of 330 g has now led this Collaboration to present the indication of a yearly signal modulation at about 2.86σ [4].

The various experimental features required for a detector to be sensitive to the expected annual-modulation effect are not met by most of the other direct detection experiments running at present. However, it is intriguing that two of them (CDMS [5] and CRESST [6]) found in their data some excesses of events over what would be expected by them from backgrounds. It is also noticeable that, at least within one of the most widely considered kind of DM particles, i.e. the one with an elastic coherent interaction with the atomic nuclei of the detector material, the CDMS and CRESST excess events would fall into (or close to) the physical region singled out by the DAMA/LIBRA and CoGeNT annual-modulation results.

The XENON100 Collaboration [7] and the CDMS Collaboration (in reanalyses of their previous data [8]) claim upper bounds—under a single set of fixed assumptions—as in conflict with the aforementioned results of the other experiments. However, problems related to the conclusions of Refs. [7,8], as discussed in Refs. [9,10] and in Ref. [11], respectively, and the existence of many uncertainties in the procedures applied in the data handling by those experiments, lead us to carry out here an analysis of the results of Refs. [3,4], not conditioned by the results reported in Refs. [7,8].

Though the model-independent annual-modulation measured in the experiments of Refs. [3,4] can be accounted for by a variety of interaction mechanisms of relic particles with the detectors materials [12], we limit our analysis here to the case where the signal is caused by nuclear recoils induced by elastic coherent interactions with the DM particles. For simplicity as in a commonly used nomenclature, in the following we will call a generic particle with these features a weakly interacting massive particle (WIMP), although the term WIMP identifies a class of DM particles which can have well different phenomenologies, like e.g. a preferred interaction with electrons [13].

Thus, in Sec. II, by using the results of Refs. [3,4] we first determine what are the physical regions pertaining to the DAMA and the CoGeNT annual-modulation data in terms of the WIMP mass and of the WIMP-nucleon elastic cross section at given confidence levels. In deriving these regions we take into account the main origins of various experimental uncertainties, as well as different forms for the distribution function (DF) of DM relic particles in the galactic halo [14].

Subsequently in Sec. III we show how the annual-modulation regions are well fitted by light neutralinos within the effective minimal supersymmetric extension of the standard model (MSSM) at the electroweak (EW) scale introduced in Ref. [15]. The relevance of light neutralinos in connection with the DAMA annual-modulation effect was first discussed in Ref. [16]; their phenomenology was then developed in the context of direct [17,18] and indirect [19] searches of DM particles. The features of this specific realization of MSSM, dubbed light neutralino model (LNM), are also confronted here with the most recent constraints on supersymmetry (SUSY) derived at the Tevatron and at the Large Hadron Collider (LHC).

Particle-physics models different from the LNM and potentially capable of generating light-WIMP particle candidates compatible with direct detection include supersymmetric models which extend the MSSM by enlarging the particle field content, like in the next-to-minimal models [20], sneutrino dark matter models [21], mirror-dark matter models [22], models with asymmetric dark matter [23], isospin-violating models [24], singlet dark matter models [25], specific realizations of grand unification [26], Higgs-portal models [27], composite models [28], specific two-Higgs doublet models [29], and secluded WIMPs [30]. Additional recent analyses can be found in Ref. [31].

Conclusions of our analysis are drawn in Sec. V.

II. REGIONS RELATED TO THE ANNUAL-MODULATION EFFECT IN CASE OF WIMPS

All experimental results discussed in the present Section are given in terms of plots in the plane m_χ–$\xi\sigma_{\rm scalar}^{\rm (nucleon)}$, where $\sigma_{\rm scalar}^{\rm (nucleon)}$ is the WIMP-nucleon cross section, $\xi = \rho_\chi/\rho_0$; ρ_0 is the local total DM density and ρ_χ the local density of the DM candidate χ. In the present Section χ denotes a generic WIMP candidate, mainly responsible for the annual-modulation effect under discussion; it will specifically denote a neutralino in the Sections to follow. The factor ξ leaves open the possibility that the considered DM candidate does not provide the total amount of local DM density.

A. Phase-space distribution functions of dark matter

The quantity $\xi\sigma_{\rm scalar}^{\rm (nucleon)}$ can be derived from the experimental spectra, once a specific DF is selected to describe the phase-space distribution function of the DM particle in the galactic halo. The appropriate form for the DF is still the subject of extensive astrophysical investigation. It is also possible that DM direct detection might be affected by the presence of unvirialized components (see, for instance, Ref. [32]). Here we have taken a few samples of DFs, selected from the various realizations examined in Ref. [14], specifically, i) the isothermal sphere (A0), ii) the Jaffe distribution (A4) [33], iii) a triaxial distribution (D2) [34] (the notation adopted here follows those of Ref. [14], to which we refer for further details). Notice that one could also have DF with a nonisotropic velocity dispersion (like distribution D2) and corotating or counter-rotating halos. Then, though the variety of DFs discussed in this paper already offer a significant sample of DFs, this selection is clearly not (and could not be) exhaustive of all possible situations.

As for the main parameters characterizing the various DFs (the local total DM density ρ_0 and the local rotational velocity v_0), we will take into account their physical ranges as discussed in Ref. [14]. Thus, we will take as representative values of v_0 either one of the two extreme values or the central value of the physical range $170\ {\rm km\,sec^{-1}} \leq v_0 \leq 270\ {\rm km\,sec^{-1}}$. For each representative value of v_0 we take for ρ_0 either its minimal $\rho_0^{\rm min}$ or its maximal value $\rho_0^{\rm max}$, in the range compatible with the given value of v_0. As in Ref. [14], $\rho_0^{\rm min}$ ($\rho_0^{\rm max}$) is defined as the value to be associated to ρ_0 when the visible mass provides its maximal (minimal) contribution to the total mass budget of the halo compatibly with observations. The numerical values for $\rho_0^{\rm min}$ and $\rho_0^{\rm max}$ depending on the DF and the values of v_0 will be taken from Table III of Ref. [14]. The escape velocity will be set at $v_{\rm esc} = 650\ {\rm km\,sec^{-1}}$.

B. Annual-modulation regions in the considered model framework

The about 9σ C.L. model independent positive results of the DAMA/NaI and DAMA/LIBRA experiments [3,35–37] and the recent positive hints by CoGeNT at 2.86σ C.L. [4] can be analyzed in many corollary model-dependent analyses. In all cases, many uncertainties in experimental parameters as well as in necessary assumptions on various related astrophysical, nuclear and particle-physics aspects must be taken into account. In the particular case of the WIMPs treated in this paper many sources of uncertainties exist; some of them have been addressed e.g. in Refs. [35,36,38]. These affect all the results at various extent both in terms of exclusion plots and in terms of allowed regions/volumes and thus comparisons with a fixed set of assumptions and parameters values are intrinsically strongly uncertain. In the following we will point out the effect of just one experimental parameter, the quenching factor, whose precise determination is quite difficult for all kinds of used detectors.

In fact, generally the direct measurements of quenching factors are performed with reference detectors, and—in some cases—with reference detectors with features quite different from the running conditions; in some other cases, these quenching factors are not even measured at all. Moreover, the real nature of these measurements and the used neutron beam/sources may not point out all the possible contributions or instead may cause uncertainties because e.g. of the presence of spurious effects due to interactions with dead materials as e.g. housing or

cryogenic assembling, if any; therefore, they are intrinsically more uncertain than generally derived. Thus, we specialize the present section to discuss the case of the values of the quenching factor of Na and I in the highly radiopure NaI(Tl) detectors of the DAMA experiments; analogous / similar discussions should be pursued for the other cases.

As is widely known, the quenching factor is a specific property of the employed detector(s) and not a general quantity universal for a given material. For example, in liquid noble-gas detectors, it depends, among other things, on the level of trace contaminants which can vary in time and from one liquefaction process to another, on the cryogenic microscopic conditions, etc.; in bolometers it depends for instance on specific properties, trace contaminants, cryogenic conditions, etc. of each specific detector, while generally it is assumed exactly equal to unity. In scintillators, the quenching factor depends, for example, on the dopant concentration, on the growing method/ procedures, on residual trace contaminants, etc., and is expected to have energy dependence. Thus, all these aspects are already by themselves relevant sources of uncertainties when interpreting whatever result in terms of DM candidates inducing just recoils as those considered in the present paper. Similar arguments have already been addressed e.g. in Refs. [3,35,36,38]. In the following, we will mention some arguments for the case of NaI(Tl), drawing the attention to the case of DAMA implications in the scenario considered in this paper.

The values of the Na and I quenching factors used by DAMA in the corollary model-dependent calculations relative to candidates inducing just recoils had, as a first reference, the values measured in Ref. [39]. This measurement was performed with a small NaI(Tl) crystal irradiated by a ^{252}Cf source, by applying the same method previously employed in Ref. [40]. Quenching factors equal to (0.4 ± 0.2) for Na and (0.05 ± 0.02) for I (integrated over the 5–100 keV and the 40–300 keV recoil energy range, respectively) were obtained. Using the same parametrization as in Ref. [40], DAMA measured in Ref. [39] quenching factors equal to 0.3 for Na and 0.09 for I, integrated over the 6.5–97 keV and the 22–330 keV recoil energy ranges, respectively. The associated errors derived from the data were quoted as one unity in the least significative digit. Then, considering also both the large variation available in the literature (see e.g. Table X of Ref. [35]) and the use of a test detector [35], a 20% associated error has been included. Nevertheless, some recent considerations, as those reported in Ref. [41] about the energy dependence of quenching factors for various recoiling ions in the same detector, have called our attention to the fact that the large uncertainties in the determination of Ref. [40] could be due, in a significant part, to uncertainties in the parametrization itself, which we also adopted. Another uncertainty could arise from the determination of integrated values, while an increase of the quenching factor values towards lower energies could be expected, as observed in some crystal detectors as for instance CsI.

An additional argument on uncertainties on quenching factors in crystals, and specifically for NaI(Tl), is the presence and the amount of the well known channeling effect of low energy ions along the crystallographic axes and planes of NaI(Tl) crystals. Such an effect can have a significant impact in the corollary model dependent analyses, in addition to those uncertainties discussed above and later on, since a fraction of the recoil events would have a much larger quenching factor than that derived with neutron calibrations. Since the channeling effect cannot be generally put into evidence with neutron measurements, as discussed in details in Ref. [38], only theoretical modeling has been produced up to now. In particular, the modeling of the channeling effect described by DAMA in Ref. [38] is able to reproduce the recoil spectrum measured at neutron beam by some other groups [42]. For completeness, we mention alternative channeling models, as that of Ref. [43], where larger probabilities of the planar channeling are expected. Moreover, we mention the analytical calculation claiming that the channeling effect holds for recoils coming from outside a crystal and not from recoils produced inside it, due to the blocking effect [44]. Nevertheless, although some amount of blocking effect could be present, the precise description of the crystal lattice with dopant and trace contaminants is quite difficult and analytical calculations require some simplifications which can affect the result.

Recently, Ref. [41] pointed out the possibility that the quenching factors for nuclear recoils in scintillators can be described with a semiempirical formula having only one free parameter: the Birks constant, k_B, which depends on the specific setup. Applying this procedure to the DAMA detectors operating underground and fixing the k_B parameter to the value able to reproduce the light response to alpha particles in these detectors, the expected Na and I quenching factors are established as a function of the energy with values ranging from 0.65 to 0.55 and from 0.35 to 0.17 in the 2–100 keV electron equivalent energy interval for Na and I nuclear recoils, respectively; as evident, also an energy dependence is pointed out there.

In the following analysis, we present some of the many possible model-dependent analyses of the DAMA results, including at least some of the present uncertainties. In particular, the uncertainties due to the description of the halo are accounted for some of the many possible halo models; we employ here the DFs mentioned in Sec. II A.

Figures 1–3 show $\xi\sigma_{\rm scalar}^{\rm (nucleon)}$ as a function of the dark matter particle mass m_χ for the A0, A4, and D2 halo models [14]. In order to have a significative sample in terms of the physical ranges of the relevant astrophysical

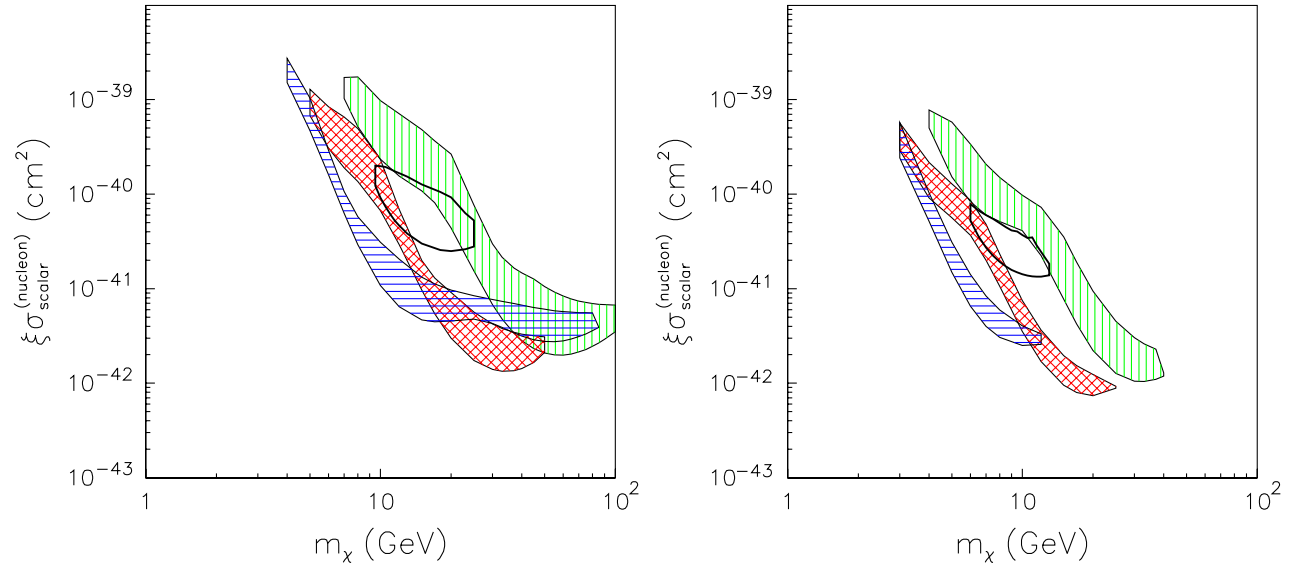

FIG. 1 (color online). $\xi\sigma^{(\mathrm{nucleon})}_{\mathrm{scalar}}$ as a function of the mass m_χ of a generic DM particle which interacts with nuclei by an elastic coherent scattering. The halo DF is taken to be given by the isothermal sphere [(A0) in the notations of Sec. II A and Ref. [14]]. The parameters are i) in the left panel, $v_0 = 170$ km sec^{-1}, $\rho_0 = 0.18$ GeV cm^{-3}, ii) in the right panel, $v_0 = 270$ km sec^{-1}, $\rho_0 = 0.45$ GeV cm^{-3} (see text for further details). The three (colored) hatched regions denote the DAMA annual-modulation regions, under the hypothesis that the effect is due to a WIMP with a coherent interaction with nuclei and in 3 different instances: i) without including the channeling effect [(green) vertically-hatched region], ii) by including the channeling effect according to Ref. [38] [(blue) horizontally-hatched region)], and iii) without the channeling effect but using the energy-dependent Na and I quenching factors as established by the procedure given in Ref. [41] [(red) cross-hatched region]. They represent the domain where the likelihood-function values differ more than 7.5σ from the null hypothesis (absence of modulation). The (nonhatched) region denoted by a (black) solid contour is the allowed region by the CoGeNT experiment when considering the modulation result given in Ref. [4] and the assumptions given in the text for the quenching factor and the form factor. This region is meant to include configurations whose likelihood-function values differ more than 1.64σ from the null hypothesis (absence of modulation). This corresponds roughly to 90% C.L. far from zero signal. In fact due to the presently more modest C.L. (about 2.9σ) of this result with respect to the 9σ C.L. of the DAMA/NaI and DAMA/LIBRA evidence for dark matter particles in the galactic halo, no region is found if the stringent 7.5σ from absence of modulation is required as for DAMA. It is worth noting that, depending on other possible uncertainties not included here, the channeled (blue) region could span the domain between the present channeled region and the unchanneled one.

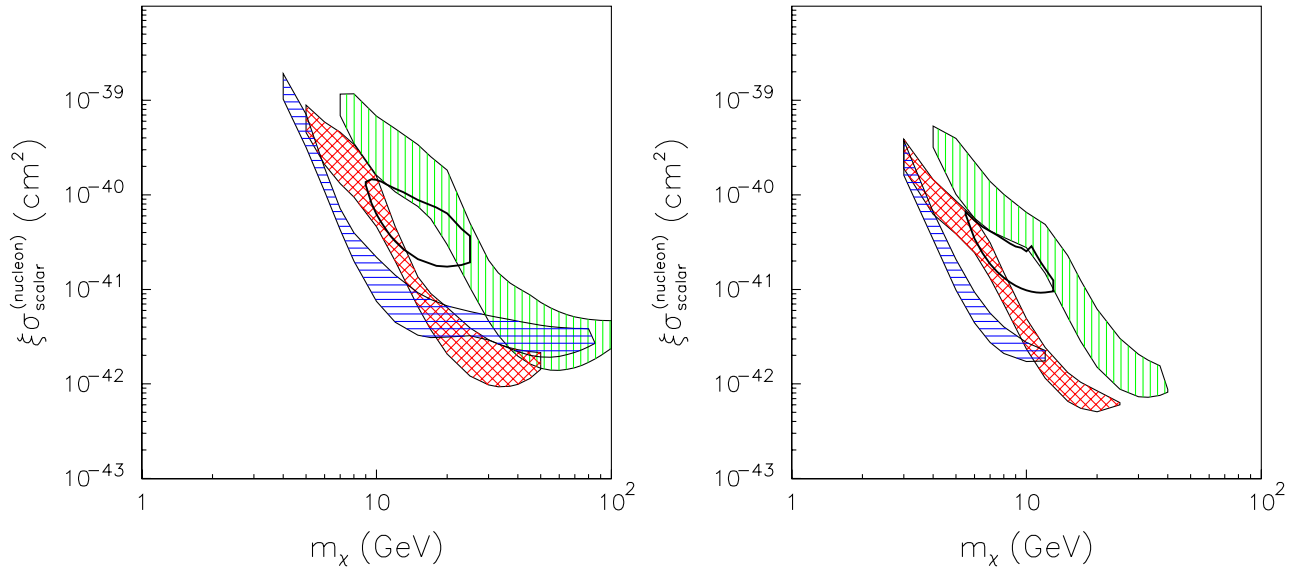

FIG. 2 (color online). As in Fig. 1 except that here the halo DF is taken to be given by the Jaffe distribution [33] [(A4) in the notations of Sec. II A and Ref. [14]]. The parameters are i) in the left panel, $v_0 = 170$ km sec^{-1}, $\rho_0 = 0.26$ GeV cm^{-3}, ii) in the right panel, $v_0 = 270$ km sec^{-1}, $\rho_0 = 0.66$ GeV cm^{-3}.

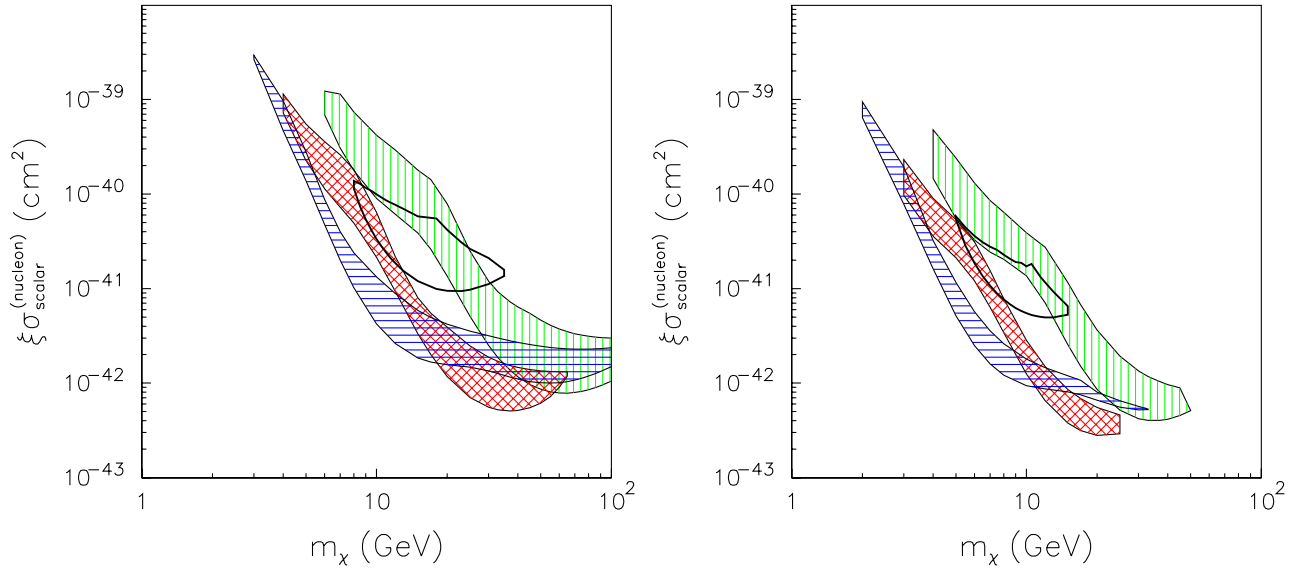

FIG. 3 (color online). As in Fig. 1 except that here the halo DF is taken to be given by a triaxial distribution [34] [(D2) in the notations of Sec. II A and Ref. [14]]. The parameters are i) in the left panel, $v_0 = 170$ km sec^{-1}, $\rho_0 = 0.50$ GeV cm^{-3}, ii) in the right panel, $v_0 = 270$ km sec^{-1}, $\rho_0 = 1.27$ GeV cm^{-3}.

parameters we have chosen to display the annual-modulation regions for the two extreme values of the local rotational velocity v_0, i.e.: $v_0 = 170$ km sec^{-1} (in the left panel of each figure) and $v_0 = 270$ km sec^{-1} (in the right panel). In Fig. 1, where the case of the A0 distribution function is shown, we have set the local total DM density ρ_0 to be equal to its minimal value, $\rho_0 = \rho_0^{\min}$, compatibly with the value of v_0, then $\rho_0 = 0.18$ GeV cm^{-3} for $v_0 = 170$ km sec^{-1} (in the left panel) and $\rho_0 = 0.45$ GeV cm^{-3} for $v_0 = 270$ km sec^{-1} (in the right panel). In Fig. 2, where we display the case of the A4 distribution function, we set again $\rho_0 = \rho_0^{\min}$, then $\rho_0 = 0.26$ GeV cm^{-3} for $v_0 = 170$ km sec^{-1} (in the left panel) and $\rho_0 = 0.66$ GeV cm^{-3} for $v_0 = 270$ km sec^{-1} (in the right panel). Figure 3 shows the case for the D2 distribution function for a value of ρ_0 equal to its maximal value, $\rho_0 = \rho_0^{\max}$; thus, $\rho_0 = 0.50$ GeV cm^{-3} for $v_0 = 170$ km sec^{-1} (in the left panel) and $\rho_0 = 1.27$ GeV cm^{-3} for $v_0 = 270$ km sec^{-1} (in the right panel). The values for $\rho_0^{\min}$ and $\rho_0^{\max}$ employed here are taken from Table III of Ref. [14]. A further example of annual-modulation regions, corresponding to the standard DF, the cored-isothermal sphere A0 with $\rho_0 = 0.34$ GeV cm^{-3} and $v_0 = 220$ km sec^{-1}, will be given in Fig. 6 in Sec. IV, where we compare the LNM with the experimental results. In all figures the escape velocity has been maintained at the fixed value: 650 km/s. Of course, the present existing uncertainties affecting the knowledge of the escape velocity—as well as other uncertainties not included here—would significantly modify/extend the allowed regions.

The three (colored) hatched regions in Figs. 1–3 denote the DAMA annual-modulation regions, under the hypothesis that the effect is due to a WIMP with a coherent interaction with nuclei and in 3 different instances: i) without including the channeling effect [(green) vertically-hatched region], ii) by including the channeling effect according to Ref. [38] [(blue) horizontally-hatched region], and iii) without the channeling effect but using an energy-dependent Na and I quenching factors as established by the procedure given in Ref. [41] [(red) cross-hatched region]. It is worth noting that, depending on the possible amount of blocking effect in NaI(Tl) with respect to the modeling used in Ref. [38], the channeled (blue) region will span the domain between the present channeled region and the unchanneled one. Moreover, the availability of quenching factor values not integrated over a large energy interval can also play a relevant role.

All these DAMA regions have been investigated here in some specific cases by adopting a procedure that allows to put into evidence—to some extent—the uncertainties on the quenching factors and on the nuclear form factors: by considering the mean values of the parameters of the used nuclear form factors and of the quenching factors of Ref. [39] (case A); by varying the mean values of those quenching factors up to $+2$ times the errors quoted there and the nuclear radius, r_n, and the nuclear surface thickness parameter, s, in the SI form factor from their central values down to -20% (case B); by fixing the Iodine nucleus parameters at the values of case B, while for the sodium nucleus one considers the quenching factor at the lowest value measured in the literature and the nuclear radius, r_n, and the nuclear surface thickness parameter, s, in the SI form factor from their central values up to $+20\%$ (case C).

The DAMA regions have been obtained by superposition of the three regions corresponding to the cases A, B, and C. These regions represent—as in some previous DAMA publications—the domain where the likelihood-function values differ more than 7.5σ from the null hypothesis (absence of modulation). This choice allows both a direct superposition of the obtained results for both Na and I target nuclei (which case by case can have different levels of the corresponding minimum value of the likelihood function) and a very high C.L. requirement.

In the same figures Figs. 1–3 the allowed regions by the CoGeNT experiment [4] (under the same adopted framework) are reported, assuming for simplicity for the Ge a fixed value of 0.2 for the quenching factor and a Helm form factor with fixed parameters. In particular, the CoGeNT regions have been obtained by fitting the measured modulation amplitudes with the WIMP expectation (S_m) and using the 0.45–3.15 keV energy region (R in the following) of the energy spectrum as a constraint. The χ^2 function is

$$\chi^2 = \sum_{k=1,2} \frac{(S_{m,k} - A_k)^2}{\sigma_{A,k}^2} + \sum_R \frac{(S_{0,k} - r_k)^2}{\sigma_k^2} \Theta(S_{0,k} - r_k), \tag{1}$$

where A_k and $\sigma_{A,k}$ are the modulation amplitudes and their errors in the two considered energy bins; r_k and σ_k are the rates and their errors in the k energy bin. The Θ Heaviside function occurs in the second term to account for the constraint of the rate in those energy bins (R). In particular, we derived from Ref. [4] the following modulation amplitudes: $A(0.5\text{–}0.9)\,\text{keV} = (0.91 \pm 0.61)\,\text{cpd/kg/keV}$; $A(0.5\text{–}3.0)\,\text{keV} = (0.45 \pm 0.18)\,\text{cpd/kg/keV}$. Thus, we consider in Eq. (1) $A_{k=1} = A(0.5\text{–}0.9)\,\text{keV}$, and we infer $A_{k=2} = A(0.9\text{–}3.0)\,\text{keV} = (0.36 \pm 0.18)\,\text{cpd/kg/keV}$. The values of the modulation amplitudes have been obtained here under the assumption that the period, and the phase of the modulation are fixed at their nominal values of 1 yr and June 2nd. If one allows the phase and the period to be free parameters, the ensuing modulation amplitudes occur to be larger but still compatible within the quoted errors.

The (nonhatched) regions denoted by (black) solid contours in Figs. 1–3 denote the allowed regions by the CoGeNT experiment; such regions contain configurations whose likelihood-function values differ more than 1.64σ from the null hypothesis (absence of modulation). This corresponds roughly to 90% CL far from zero signal. In fact due to the presently more modest C.L. (about 2.9σ) of the CoGeNT result with respect to the 9σ C.L. of the DAMA/NaI and DAMA/LIBRA evidence for DM particles in the galactic halo, obviously no region is found if the stringent 7.5σ from absence of modulation is required as for the DAMA cases; thus, it will be very interesting to see future CoGeNT data releases with increased significance. Anyhow, all the examples given here, as well as the proper inclusion of possible uncertainties in the assumptions adopted for CoGeNT and additional accounting of other uncertainties, offer a substantial agreement between the two experiments (as well as with some preliminary possible positive hint by CRESST discussed at Conferences so far [6], which is not addressed here) towards a low mass candidate.

From Figs. 1–3 we see that in all instances the DAMA and the CoGeNT regions agree quite well, over ranges of $\xi\sigma_{\text{scalar}}^{(\text{nucleon})}$ and m_χ somewhat wider as compared to those derived for instance in Refs. [4,45]. The gross features in the comparative positions of the various regions in our Figs. 1–3 are easily understood in terms of the specific values of the DF parameters employed. Further statistics in the CoGeNT experiment will be useful in pinning down more precisely the common domains for the two annual-modulation experiments.

III. THE LIGHT NEUTRALINO MODEL

Now we discuss how the results reported in the previous Section are well fitted by the light neutralinos which arise within the model introduced in Ref. [15] and developed in the papers of Ref. [17]. Lately, this model, denoted as Light Neutralino Model (LNM), was updated in Refs. [18,46] to take into account recent constraints on supersymmetric models derived at accelerators and B factories.

A. Main features of the LNM

The LNM is an effective MSSM scheme at the electroweak scale with the following independent parameters: M_1, M_2, M_3, μ, $\tan\beta$, m_A, $m_{\tilde{q}}$, $m_{\tilde{l}}$, and A. Notations are as follows: M_1, M_2, and M_3 are the U(1), SU(2), and SU(3) gaugino masses (these parameters are taken here to be positive), μ is the Higgs mixing mass parameter, $\tan\beta$ the ratio of the two Higgs vacuum expectation values, m_A the mass of the CP-odd neutral Higgs boson, $m_{\tilde{q}}$ is a squark soft mass common to the all families, $m_{\tilde{l}}$ is a slepton soft mass common to all sleptons, and A is a common dimensionless trilinear parameter for the third family, $A_{\tilde{b}} = A_{\tilde{t}} \equiv Am_{\tilde{q}}$ and $A_{\tilde{\tau}} \equiv Am_{\tilde{l}}$ (the trilinear parameters for the other families being set equal to zero). We recall that in Ref. [46] the possibility of a splitting between the squark soft mass common to the first two families and that of the third family was considered. This allows to reduce the fine tuning in the parameters that can be induced by the interplay between the constraint from the $b \to s\gamma$ decay and those from SUSY searches at the LHC.

The linear superposition of bino $\tilde{B}$, wino $\tilde{W}^{(3)}$, and of the two Higgsino states $\tilde{H}_1^\circ$, $\tilde{H}_2^\circ$ which defines the neutralino state of lowest mass m_χ will be written here as

$$\chi \equiv a_1\tilde{B} + a_2\tilde{W}^{(3)} + a_3\tilde{H}_1^\circ + a_4\tilde{H}_2^\circ. \tag{2}$$

Since no gaugino-mass unification at a Grand Unified scale is assumed in our LNM (at variance with one of the major assumptions in mSUGRA), in this model

the neutralino mass is not bounded by the lower limit $m_\chi \gtrsim 50$ GeV that is commonly derived in mSUGRA schemes from the LEP lower bound on the chargino mass (of about 100 GeV). In Refs. [15–18] it is shown that, if R parity is conserved, a light neutralino (i.e. a neutralino with $m_\chi \lesssim 50$ GeV) is a very interesting candidate for cold dark matter (CDM), due to its relic abundance and its relevance in the interpretation of current experiments of search for relic particles; it is also shown there that a lower bound $m_\chi \gtrsim 7$–8 GeV is obtained from the cosmological upper limit on CDM. The compatibility of these results with all experimental searches for direct or indirect evidence of SUSY (prior to the first physics results of LHC) and with other precision data that set constraints on possible effects due to supersymmetry is discussed in detail in Ref. [18]. The viability of very light neutralinos in terms of various constraints from collider data, precision observables and rare meson decays is also considered in Ref. [47]. Perspectives for investigation of these neutralinos at the International Linear Collider (LHC) are analyzed in Ref. [48] and prospects for a very accurate mass measurement at ILC in Ref. [49].

In the present section we essentially recall the main properties of the light neutralinos within the LNM, as derived in Refs. [15–18], and which are relevant for the discussion of the experimental results of Refs. [3,4].

In the regime of light neutralinos the lower limit on the mass m_χ, obtained from the requirement that its relic abundance does not exceed the observed upper bound for cold dark matter (CDM), i.e. $\Omega_\chi h^2 \leq (\Omega_{\rm CDM} h^2)_{\rm max}$, can be expressed analytically in terms of the relevant SUSY parameters. In this concern, it is convenient to distinguish between two scenarios. The first one is denoted as Scenario $\mathcal{A}$, and its main features are: i) m_A is light, 90 GeV $\leq m_A \lesssim$ (200–300) GeV (90 GeV being the lower bound from LEP searches); ii) $\tan\beta$ is large: $\tan\beta = 20$–45, iii) the $\tilde{B} - \tilde{H}_1^\circ$ mixing needs to be sizeable, which in turn implies small values of μ: $|\mu| \sim$ (100–200) GeV. In this scenario the dominant contribution to the annihilation cross section of a pair of neutralinos, $\sigma_{\rm ann}$ (which establishes the size of the neutralino relic abundance) is provided by the A exchange in the s channel of the annihilation process $\chi + \chi \to \bar{b} + b$, thus the lower bound on m_χ is given by

$$m_\chi \frac{[1 - m_b^2/m_\chi^2]^{1/4}}{[1 - (2m_\chi)^2/m_A^2]} \gtrsim 7.4 \text{ GeV} \left(\frac{m_A}{90 \text{ GeV}}\right)^2 \left(\frac{35}{\tan\beta}\right) \times \left(\frac{0.12}{a_1^2 a_3^2}\right)^{1/2} \left(\frac{0.12}{(\Omega_{\rm CDM} h^2)_{\rm max}}\right)^{1/2}, \quad (3)$$

where m_b is the mass of the b quark.

When $m_A \gtrsim$ (200–300) GeV, the cosmological upper bound on the neutralino relic abundance can be satisfied by a pair annihilation process which proceeds through an efficient stau-exchange contribution (in the t, u channels). This requires that (i) the stau mass $m_{\tilde{\tau}}$ is sufficiently light, $m_{\tilde{\tau}} \sim 90$ GeV (notice that the current experimental limit is $m_{\tilde{\tau}} \sim 87$ GeV) and (ii) χ is a very pure bino [i.e. $(1 - a_1^2) \sim \mathcal{O}(10^{-2})$]. Thus, one is lead to a Scenario $\mathcal{B}$, identified by the following sector of the supersymmetric parameter space: $M_1 \sim 25$ GeV, $|\mu| \gtrsim 500$ GeV, $\tan\beta \lesssim 10$; $m_{\tilde{l}} \gtrsim$ (100–200) GeV, $-2.5 \lesssim A \lesssim +2.5$. As derived in Ref. [15–18], in this scenario the cosmological bound $\Omega_\chi h^2 \leq (\Omega_{\rm CDM} h^2)_{\rm max}$ provides the lower bound $m_\chi \gtrsim 22$ GeV [50], whose scaling law in terms of the stau mass and $(\Omega_{\rm CDM} h^2)_{\rm max}$ is approximately given by

$$m_\chi [1 - m_{\tilde{\tau}}^2/m_\chi^2]^{1/4} \gtrsim 22 \text{ GeV} \left(\frac{m_{\tilde{\tau}}}{90 \text{ GeV}}\right)^2 \times \left(\frac{0.12}{(\Omega_{\rm CDM} h^2)_{\rm max}}\right). \quad (4)$$

In Scenario $\mathcal{A}$ the neutralino-nucleon cross section $\sigma_{\rm scalar}^{\rm (nucleon)}$ is dominated by the interaction process due to the exchange of the lighter CP-even neutral Higgs boson h, whose mass m_h has a numerical value very close to m_A; then $\sigma_{\rm scalar}^{\rm (nucleon)}$ is expressible as

$$\sigma_{\rm scalar}^{\rm (nucleon)} \simeq 5.3 \times 10^{-41} \text{ cm}^2 \left(\frac{a_1^2 a_3^2}{0.13}\right) \left(\frac{\tan\beta}{35}\right)^2 \left(\frac{90 \text{ GeV}}{m_h}\right)^4 \times \left(\frac{g_d}{290 \text{ MeV}}\right)^2, \quad (5)$$

where g_d is the dominant coupling in the interaction of the Higgs-boson h with the d-type quarks,

$$g_d \equiv [m_d \langle N|\bar{d}d|N\rangle + m_s \langle N|\bar{s}s|N\rangle + m_b \langle N|\bar{b}b|N\rangle], \quad (6)$$

and $\langle N|\bar{d}d|N\rangle$ denotes the scalar density of a generic quark q inside the nucleon. In this expression we have used as *reference* value for g_d the value $g_{d,\rm ref} = 290$ MeV employed in our previous papers [17]. We recall that this quantity is affected by large uncertainties [51] with $(g_{d,\rm max}/g_{d,\rm ref})^2 = 3.0$ and $(g_{d,\rm min}/g_{d,\rm ref})^2 = 0.12$, a fact that directly transforms in the same amount of uncertainty on the coherent scattering cross section.

Since, as mentioned in Sec. II, we wish to consider also situations where relic neutralinos only provide a fraction of the CDM abundance, the relevant quantity we will compare with the experimental results is not simply $\sigma_{\rm scalar}^{\rm (nucleon)}$ but rather $\xi \sigma_{\rm scalar}^{\rm (nucleon)}$. The factor $\xi = \rho_\chi/\rho_0$ is calculated here according to the *rescaling* recipe $\xi = \min\{1, \Omega_\chi h^2/(\Omega_{\rm CDM} h^2)_{\rm min}\}$ [52], where $(\Omega_{\rm CDM} h^2)_{\rm min}$ is the minimal value to be assigned to the relic abundance of CDM.

It is remarkable that for neutralino configurations, *whose relic abundance stays in the cosmological range for CDM* [i.e. $(\Omega_{\rm CDM} h^2)_{\rm min} \leq \Omega_\chi h^2 \leq (\Omega_{\rm CDM} h^2)_{\rm max}$ with $(\Omega_{\rm CDM} h^2)_{\rm min} = 0.098$ and $(\Omega_{\rm CDM} h^2)_{\rm max} = 0.12$] and pass all particle-physics constraints, the elastic neutralino-nucleon cross section can be cast as [15–18]

$$\sigma_{\rm scalar}^{\rm (nucleon)} \simeq (2.7\text{–}3.4)\times 10^{-41}\ {\rm cm}^2\left(\frac{g_d}{290\ {\rm MeV}}\right)^2 \times \frac{[1-(2m_\chi)^2/m_A^2]^2}{(m_\chi/(10\ {\rm GeV})^2[1-m_b^2/m_\chi^2]^{1/2}}. \quad (7)$$

Notice that this formula provides an evaluation of $\sigma_{\rm scalar}^{\rm (nucleon)}$ simply in terms of the neutralino mass m_χ. Specific SUSY parameters such as $\tan\beta$ or μ do not appear explicitly, since these parameters have been reabsorbed by the introduction of the relic abundance (this is because here the annihilation amplitude is related to the elastic-scattering amplitude by crossing symmetry). The remaining dependence on the mass of the interaction mediator $m_A \simeq m_h$ is only marginal, due to the small values of m_χ considered here.

Equation (7) is of particular interest in establishing the range of values for $\sigma_{\rm scalar}^{\rm (nucleon)}$ in terms of the neutralino mass. The numerical range in front of Eq. (7) follows from the requirement that relic neutralinos have an abundance in the cosmological range for CDM. The crucial factor of uncertainties in $\sigma_{\rm scalar}^{\rm (nucleon)}$ is related to QCD properties through the coupling g_d. It is however worth recalling that the range of the neutralino mass depends on the lower bound on m_χ which is explicitly given in terms of the SUSY parameters in Eq. (3). These properties will also show up later in the figures displaying the scatter plots for $\sigma_{\rm scalar}^{\rm (nucleon)}$.

B. Constraints on SUSY parameters from early searches at the LHC

In Ref. [46] the possible impact of some early analyses by the CMS and ATLAS Collaborations at the LHC on the LNM was investigated. The data considered there consisted in the results of searches for supersymmetry in proton-proton collisions at a center-of-mass energy of 7 TeV with an integrated luminosity of 35 pb^{-1} [53], i.e. the results of the CMS Collaboration for events with jets and missing transverse energy [53] and those of the ATLAS Collaboration by studying final states containing jets, missing transverse energy, either with a isolated lepton (electron or muon) [54] or without final leptons [55]. Both signatures would be significant of processes due to the production in pairs of squarks and gluinos, subsequently decaying into quarks, gluons, other standard-model (SM) particles and a neutralino [interpreted as the lightest supersymmetric particle (LSP)] in an R parity conserving SUSY theory. As reported in Refs. [53,54] the data appeared to be consistent with the expected SM backgrounds; thus lower bounds were derived on the squark and gluino masses which are sizably higher than the previous limits established by the experiments D0 [56] and CDF [57] at the Tevatron.

These data were employed in Ref. [46] to determine the relevant lower bounds on the squark masses and the gluino mass M_3 within the LNM and their ensuing possible impact on the value of the lower bound on the neutralino mass. It was proved there that the data of Refs. [53,54] do not imply a modification of the lower bound $m_\chi \gtrsim$ 7–8 GeV for the LNM when the common squark mass for the first two families $m_{\tilde{q}_{12}}$ and the one for the third family $m_{\tilde{t}}$ are independent parameters with $m_{\tilde{q}_{12}} > m_{\tilde{t}}$ or, in case of a full degeneracy of the squark masses over the 3 families (as considered in the present paper), when $M_3 \gtrsim$ (1.5–2) TeV. Otherwise, in the case of a full squark-mass degeneracy ($m_{\tilde{q}_{12}} = m_{\tilde{t}} \equiv m_{\tilde{q}}$) the lower bound on m_χ varies as a function of the gluino mass M_3, from the value of 7–8 GeV for $M_3 \gtrsim 2$ TeV to about 12 GeV for $M_3 \simeq$ 600 GeV (see Fig. 5 of Ref. [46] for details). In particular, the gluino mass enters in the calculation of observables for the relic neutralino only at the loop level (through radiative corrections of Higgs couplings), so within the LNM M_3 is very weakly correlated to the other parameters. In order to reduce the number of parameters, in the present analysis we choose to decouple the gluino mass assuming $M_3 = 2$ TeV. In this case LHC data imply the lower bound $m_{\tilde{q}} \gtrsim 450$ within the LNM [46]. In the following we will impose this constraint in our numerical analysis.

Now, we proceed to a discussion of the new results presented by the CMS Collaboration on a search for neutral SUSY Higgs bosons decaying in tau pairs at a center-of-mass energy of 7 TeV with an integrated luminosity of 36 pb^{-1} [58]. Since no excess is observed in the tau-pair invariant-mass spectrum, upper limits on the Higgs-boson production cross section times the branching ratio to tau pairs are placed. These limits are then converted into upper bounds for the SUSY parameter $\tan\beta$ as a function of the pseudoscalar Higgs-boson mass m_A in a particular MSSM benchmark. The ensuing disallowed region in the plane $m_A - \tan\beta$ turns out to be considerably larger than the one previously derived at the Tevatron (see for instance Ref. [59]).

However, in Ref. [60] it has been shown that, when all the theoretical uncertainties involved in the derivation of the previous bounds on the Higgs-boson production cross section times the branching ratio to tau pairs are appropriately taken into account, the limits on the SUSY parameters reported in Refs. [58,59] are significantly relaxed.

We display in Fig. 4 the region disallowed in the plane ($\tan\beta - m_A$) from the results of Refs. [58], as derived in the analysis of Ref. [60]. In this figure we also show the lines corresponding to fixed values of the neutralino mass in the LNM. Thus we see that the CMS upper bounds of Ref. [58] do not modify the value of the neutralino-mass lower bound $m_\chi \gtrsim$ 7–8 GeV previously derived in Refs. [17,18]. This result also follows directly from the analytic expression of Eq. (3) for the lower limit on m_χ.

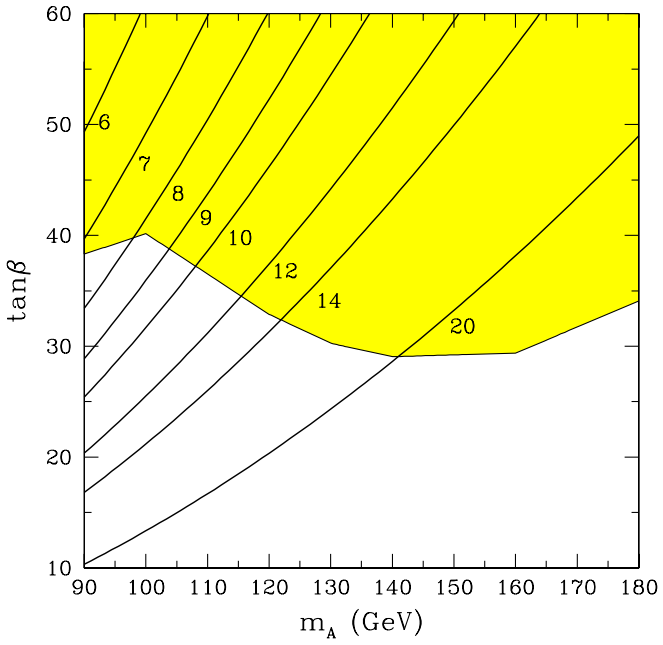

FIG. 4 (color online). Upper bounds in the m_A–tanβ plane, derived in Ref. [60] from searches of the neutral Higgs boson decaying into a tau pair at LHC [58]. The disallowed domain is the (yellow) shaded region. The solid bold lines labeled by numbers denote the cosmological bound $\Omega_\chi h^2 \leq (\Omega_{\rm CDM} h^2)_{\rm max}$ for a neutralino whose mass is given by the corresponding number (in units of GeV), as obtained by Eq. (3) with $(\Omega_{\rm CDM} h^2)_{\rm max} = 0.12$. For any given neutralino mass, the allowed region is above the corresponding line.

The predictions of the LNM for the cross section $\sigma^{(\rm nucleon)}_{\rm scalar}$ were already anticipated in the analytic expressions of Eqs. (5)–(7). Now we give the numerical values for the quantity $\xi\sigma^{(\rm nucleon)}_{\rm scalar}$ which will finally be confronted with the experimental results. Figure 5 provides the scatter plots of this quantity for the neutralino configurations which pass all the constraints previously discussed in this Section. In particular, in our scan of the LNM the following ranges of the parameters are adopted: $10 \leq \tan\beta \leq 50$, $105\ {\rm GeV} \leq \mu \leq 1000\ {\rm GeV}$, $5\ {\rm GeV} \leq M_1 \leq 50\ {\rm GeV}$, $100\ {\rm GeV} \leq M_2 \leq 2500\ {\rm GeV}$, $450\,{\rm GeV} \leq m_{\tilde q} \leq 3000\,{\rm GeV}$, $115\ {\rm GeV} \leq m_{\tilde l} \leq 3000\ {\rm GeV}$, $90\ {\rm GeV} \leq m_A \leq 1000\ {\rm GeV}$, $-3 \leq A \leq 3$.

The left panel refers to SUSY configurations with a neutralino relic abundance which matches the Wilkinson Microwave Anisotropy Probe (WMAP) cold dark matter amount ($0.098 \leq \Omega_\chi h^2 \leq 0.122$), whereas the right panel displays by (blue) dots the configurations where the neutralino is subdominant ($\Omega_\chi h^2 < 0.098$). In both panels, the flaglike region denotes the extension of the scatter plots upwards and downwards, when the hadronic uncertainties are included.

IV. COMPARISON WITH EXPERIMENTAL RESULTS

The predictions for $\xi\sigma^{(\rm nucleon)}_{\rm scalar}$ for light neutralinos within the LNM, as depicted in Fig. 5, fall clearly in the

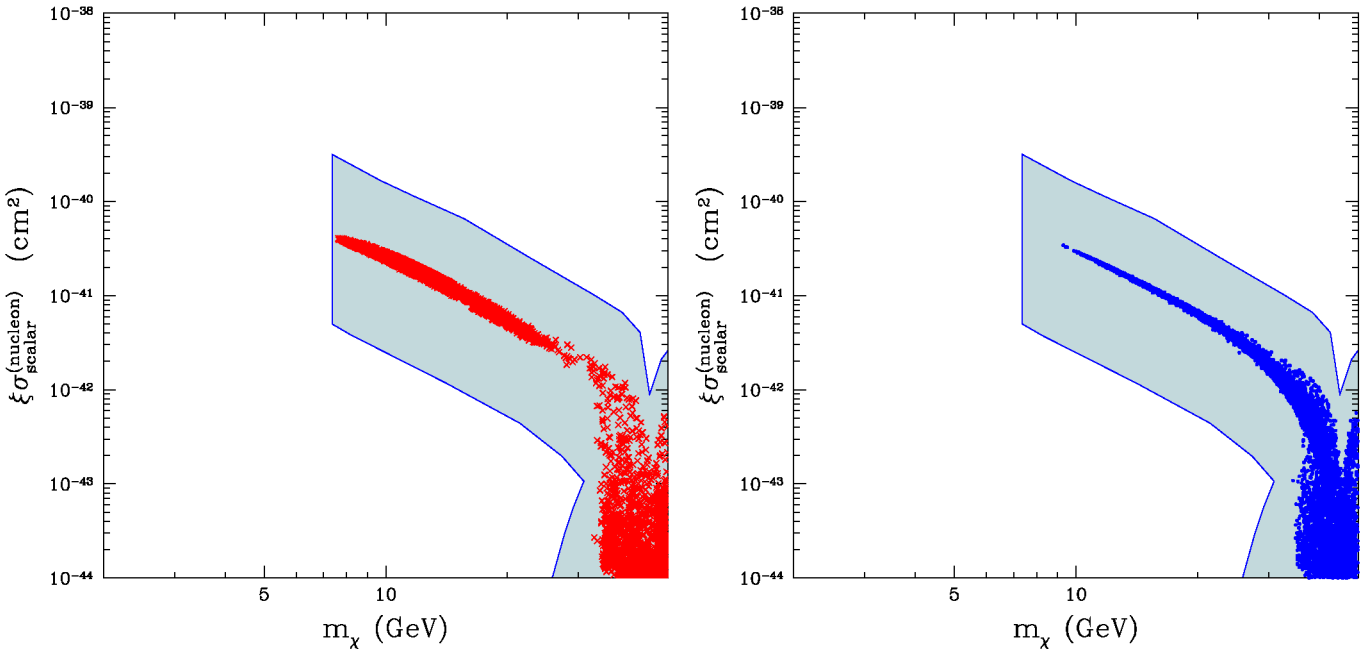

FIG. 5 (color online). Scatter plot for $\xi\sigma^{(\rm nucleon)}_{\rm scalar}$ as a function of the neutralino mass for $g_{d,\rm ref} = 290$ MeV. The left panel displays by (red) crosses SUSY configurations with a neutralino relic abundance which matches the WMAP cold dark matter amount ($0.098 \leq \Omega_\chi h^2 \leq 0.122$), whereas the right panel displays by (blue) dots the configurations where the neutralino is subdominant ($\Omega_\chi h^2 < 0.098$). The (light-blue) flaglike region denotes the extension of the scatter plot upwards and downwards when the hadronic uncertainties are included.

region of interest of the present annual-modulation results as reproduced in Figs. 1–3 and in Fig. 7 (to follow). For a more specific comparison among experiments and theory we employ here, as a reference DF, the *standard* isothermal sphere with parameters: $\rho_0 = 0.34$ GeV cm^{-3}, $v_0 = 220$ km sec^{-1}, $v_{esc} = 650$ km sec^{-1}. This choice is not meant to attribute to this particular DF a privileged role over other DFs but is done simply for convenience, to conform to the most commonly employed form of the DF. The experiment-theory comparison is therefore displayed in Fig. 6. The features of this figure confirm that the conclusions drawn in Ref. [18] are even reinforced when, as done in the present paper, the new annual-modulation results by CoGeNT are included, specifically: i) the light neutralino population agrees with the DAMA/LIBRA annual-modulation data over a wide range of light neutralinos: 7–8 GeV $\lesssim m_\chi \lesssim$ 50 GeV, ii) this population is also in agreement with the data of CoGeNT in a range of the neutralino mass somewhat restricted to the lower masses: 7–8 GeV $\lesssim m_\chi \lesssim$ (15–20) GeV.

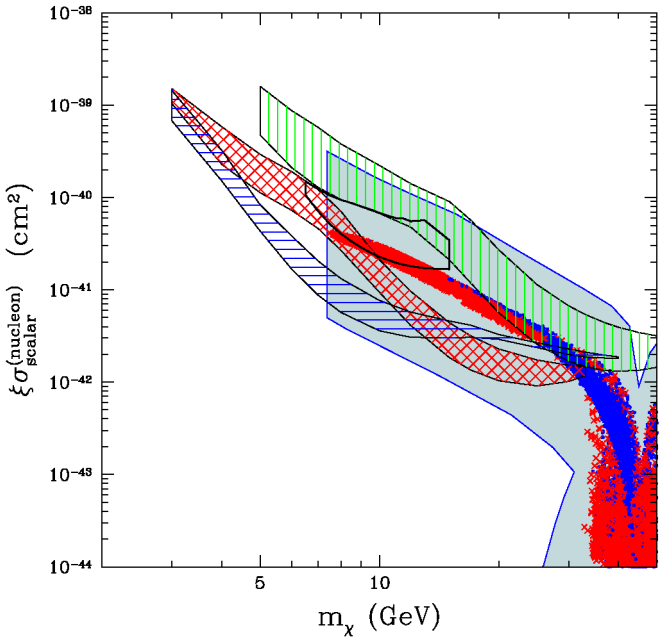

FIG. 6 (color online). $\xi\sigma^{(nucleon)}_{scalar}$ as a function of the neutralino mass. The experimental annual-modulation regions are obtained as explained in the caption of Fig. 1, except that here the used DF is an isothermal sphere with the following values for the parameters: $\rho_0 = 0.34$ GeV cm^{-3}, $v_0 = 220$ km sec^{-1}, $v_{esc} = 650$ km sec^{-1}. The theoretical scatter plot displays the whole sample of neutralino configurations: (red) crosses denote SUSY configurations with a neutralino relic abundance which matches the WMAP cold dark matter amount ($0.098 \leq \Omega_\chi h^2 \leq 0.122$), while (blue) dots denote the configurations where the neutralino is subdominant ($\Omega_\chi h^2 < 0.098$) (these two sets of configurations were shown separately in Fig. 5). The scatter plot has been evaluated for $g_{d,\mathrm{ref}} = 290$ MeV. The (light-blue) flaglike region denotes the extension of the scatter plot upwards and downwards when the hadronic uncertainties are included (see text).

It is worth recalling that also the data of CDMS [5], and CRESST [6], should their reported excesses be significant of real DM signals, would fall in a domain of the $\xi\sigma^{(nucleon)}_{scalar}$–$m_\chi$ plane overlapping with the DAMA and CoGeNT regions.

V. CONCLUSIONS

The long-standing model-independent annual-modulation signal measured by the DAMA Collaboration for a total exposure of 1.17 ton × year and a confidence level of 8.9σ with a NaI(Tl) detector [3] has been comparatively examined with the new results by the CoGeNT experiment [3] which shows a similar behavior with a statistical significance of about 2.86σ. The annual modulation measured in these two experiments is an effect expected because of the relative motion of the Earth with respect to the relic particles responsible for the dark matter in the galactic halo [1]. The underlying physical process can be due to a variety of interaction mechanisms of relic particles with the detector materials [12]. Here we have limited our analysis to the case where the signal would be caused by nuclear recoils induced by elastic coherent interactions of the target nuclei with the DM particles.

The ensuing physical regions in the plane of the DM-particle mass versus the DM-particle-nucleon cross section have been derived for a variety of DM distribution functions in the galactic halo and by taking into account the impact of various experimental uncertainties.

The phase-space distribution of DM particles in the halo is still subject of extensive astrophysical investigations, with the possible presence of unvirialized components (see, for instance, Ref. [32]). Here we have selected a few samples of DFs, selected among those discussed in Ref. [14], from the isothermal sphere to the Jaffe DF [33] to a triaxial one [34].

We have examined in details to what extent the major experimental uncertainties, most notably those related to the quenching factors and the channeling effect, affect the derivation of the annual-modulation physical regions. It is shown that the DAMA and the CoGeNT regions agree well between each other independently of the specific analytic form of the DFs considered here, considering also that some existing uncertainties have not been taken into account for the CoGeNT allowed regions. For completeness, Fig. 7 shows the DAMA allowed regions in the three considered instances for the Na and I quenching factors when including all the DFs considered in Ref. [14] and the same uncertainties as in Ref. [35,36]. The allowed region obtained for the CoGeNT experiment, including the same astrophysical models as in Ref. [35,36] and assuming for simplicity a fixed value for the Ge quenching factor and a Helm form factor with fixed parameters, is also reported in Fig. 7 (solid line); it fully overlaps the DAMA allowed regions. The inclusion of other uncertainties on parameters

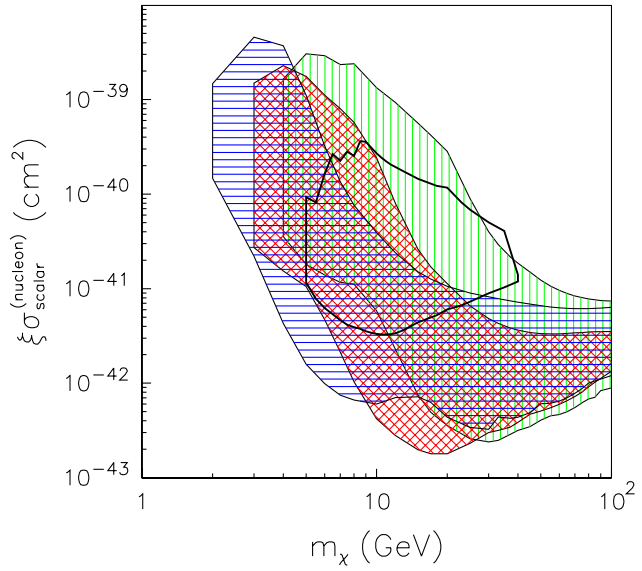

FIG. 7 (color online). Regions in the $\xi\sigma^{(\mathrm{nucleon})}_{\mathrm{scalar}}$ vs m_χ plane allowed by DAMA experiments in the three considered instances for the Na and I quenching factors, including all the DFs considered in Ref. [14] and the same uncertainties as in Refs. [35,36] for a WIMP with a pure SI coupling. The hatchings (and colors) of the allowed regions are the same as those in Fig. 1. These regions represent the domain where the likelihood-function values differ more than 7.5σ from the null hypothesis (absence of modulation). It is worth noting that, depending on other possible uncertainties not included here, the channeled (blue) horizontally-hatched region could span the domain between the present channeled region and the unchanneled one. The allowed region obtained for the CoGeNT experiment, including the same astrophysical models as in Ref. [35,36] and assuming for simplicity a fixed value for the Ge quenching factor and a Helm form factor with fixed parameters, is also reported and denoted by a (black) thick solid line. This region is meant to include configurations whose likelihood-function values differ more than 1.64σ from the null hypothesis (absence of modulation). This corresponds roughly to 90% CL far from zero signal. See text.

and models (see, for example, Refs. [35,36]) would further enlarge these regions.

In this paper, we have finally discussed a specific particle-physics realization, the Light Neutralino Model, where neutralinos with masses in the tens of GeV range naturally arise. This supersymmetric model, which was already shown [18] to be successful in fitting the DAMA annual-modulation results [3] as well as the (unmodulated) CoGeNT [61], the CDMS [5] and the CRESST [6] excesses, is shown here to agree quite well also with the most recent CoGeNT annual-modulation data [4]. Notice that the LNM discussed here satisfies all available experimental particle-physics constraints, including the most recent results from CMS and ATLAS at the CERN Large Hadron Collider. Confirmation of the validity of the SUSY model discussed in the present paper rests on the possibility of a positive evidence of light neutralinos in further running of LHC [48].

ACKNOWLEDGMENTS

The authors thank the DAMA Collaboration for making available the data for this analysis. A. B. and N. F. acknowledge Research Grants funded jointly by Ministero dell'Istruzione, dell'Università e della Ricerca (MIUR), by Università di Torino and by Istituto Nazionale di Fisica Nucleare within the *Astroparticle Physics Project* (MIUR Contract No. PRIN 2008NR3EBK; INFN Grant No. FA51). S. S. acknowledges support by NRF with CQUEST Grant No. 2005-0049049 and by the Sogang Research Grant 2010. N. F. acknowledges support of the Spanish MICINN Consolider Ingenio 2010 Programme under Grant No. MULTIDARK CSD2009- 00064.

Note added.—In this Note we comment on two preprints that appeared after the submission of the present paper.

The viability of an MSSM to obtain a neutralino-nucleon elastic cross section with a size relevant for the DAMA and CoGeNT annual-modulation data, for light neutralino masses, is questioned in the preprint of Ref. [62]. We note that in the MSSM scheme employed in Ref. [62] the squark masses are all set at 1 TeV. From the properties discussed in detail in Refs. [18,46] it is clear that taking all the squark masses at this value generates tension between the $b \to s + \gamma$ and the $B_s \to \mu^+ + \mu^-$ constraints and thus precludes low values of the Higgs-boson masses (i.e close the their LEP lower bounds). This, in turn, disallows neutralino masses $\lesssim 15$ GeV (see Fig. 2 of Ref. [46]). At variance with the conclusions of Ref. [62], in the present paper it is shown that an appropriate MSSM scheme fits the DAMA and CoGeNT annual-modulation results quite well in force of the properties spelled out in Sec. III.

Ref. [63] refers to our approach in the analysis of the CoGeNT data as being "somewhat unphysical", since, according to Ref. [63], we would accept negative backgrounds. This is manifestly not the case, as can be easily understood by means of Eq. (1), which defines the statistical estimator we use in our analysis. We explicitly enforce the bound arising from the total rate in order not to accept modulation amplitudes which would be incompatible with the measured total rate. The last term in Eq. (1) does, in fact, penalize the χ^2 when the calculated rate becomes exceedingly large, statically incompatible with the measured total rate. We therefore do not accept negative backgrounds, contrary to the claim in Ref. [63].

[1] A. K. Drukier, K. Freese, and D. N. Spergel, Phys. Rev. D **33**, 3495 (1986); K. Freese, J. Friedman, and A. Gould, Phys. Rev. D **37**, 3388 (1988).

[2] R. Bernabei *et al.*, Phys. Lett. B **C424**, 195 (1998).

[3] R. Bernabei *et al.*, Eur. Phys. J. C **56**, 333 (2008); **67**, 39 (2010).

[4] C. E. Aalseth *et al.*, arXiv:1106.0650.

[5] Z. Ahmed *et al.* (CDMS Collaboration), Science **327**, 1619 (2010); Science **327**, 1619 (2010).

[6] W. Seidel, IDM, Montpellier, France, 2010.

[7] E. Aprile *et al.* (XENON100 Collaboration), arXiv:1104.2549.

[8] D. S. Akerib *et al.*, Phys. Rev. D **82**, 122004 (2010); Z. Ahmed *et al.*, Phys. Rev. Lett. **106**, 131302 (2011).

[9] R. Bernabei, P. Belli, A. Incicchitti, and D. Prosperi, arXiv:0806.0011v2.

[10] J. I. Collar, arXiv:1106.0653.

[11] J. I. Collar, arXiv:1103.3481.

[12] R. Bernabei *et al.*, Eur. Phys. J. C **56**, 333 (2008).

[13] R. Bernabei *et al.*, Phys. Rev. D **77**, 023506 (2008), and references therein.

[14] P. Belli, R. Cerulli, N. Fornengo, and S. Scopel, Phys. Rev. D **66**, 043503 (2002).

[15] A. Bottino, N. Fornengo, and S. Scopel, Phys. Rev. D **67**, 063519 (2003); A. Bottino, F. Donato, N. Fornengo, and S. Scopel, Phys. Rev. D **68**, 043506 (2003).

[16] A. Bottino, F. Donato, N. Fornengo, and S. Scopel, Phys. Rev. D **69**, 037302 (2004).

[17] A. Bottino, F. Donato, N. Fornengo, and S. Scopel, Phys. Rev. D **77**, 015002 (2008); **78**, 083520 (2008); **81**, 107302 (2010).

[18] N. Fornengo, S. Scopel, and A. Bottino, Phys. Rev. D **83**, 015001 (2011).

[19] A. Bottino, F. Donato, N. Fornengo, and S. Scopel, Phys. Rev. D **70**, 015005 (2004); V. Niro, A. Bottino, F. Donato, N. Fornengo, and S. Scopel, Phys. Rev. D **80**, 095019 (2009).

[20] D. G. Cerdeno and O. Seto, J. Cosmol. Astropart. Phys. 08 (2009) 032; D. G. Cerdeno, C. Munoz, and O. Seto, Phys. Rev. D **79**, 023510 (2009); D. G. Cerdeno, E. Gabrielli, D. E. Lopez-Fogliani, C. Munoz, and A. M. Teixeira, J. Cosmol. Astropart. Phys. 06 (2007) 008; J. F. Gunion, A. V. Belikov, and D. Hooper, arXiv:1009.2555; A. V. Belikov, J. F. Gunion, D. Hooper, and T. M. P. Tait, arXiv:1009.0549.

[21] C. Arina and N. Fornengo, J. High Energy Phys. 11 (2007) 029; G. Belanger, S. Kraml, and A. Lessa, J. High Energy Phys. 07 (2011) 083.

[22] R. Foot, arXiv:1106.2688; Phys. Rev. D **82**, 095001 (2010); Y. Mambrini, J. Cosmol. Astropart. Phys. 07 (2011) 009; 09 (2010) 022.

[23] E. Del Nobile, C. Kouvaris, and F. Sannino, Phys. Rev. D **84**, 027301 (2011).

[24] S. Chang, J. Liu, A. Pierce, N. Weiner, and I. Yavin, J. Cosmol. Astropart. Phys. 08 (2010) 018; J. L. Feng, J. Kumar, D. Marfatia, and D. Sanford, arXiv:1102.4331v2; M. T. Frandsen, F. Kahlhoefer, J. March-Russell, C. McCabe, M. McCullough, and K. Schmidt-Hoberg, arXiv:1105.3734.

[25] Y. G. Kim and S. Shin, J. High Energy Phys. 05 (2009) 036; S. Shin, arXiv:1011.6377.

[26] M. R. Buckley, D. Hooper, and J. L. Rosner, arXiv:1106.3583.

[27] S. Andreas *et al.*, Phys. Rev. D **82**, 043522 (2010); S. Andreas, T. Hambye, and M. H. G. Tytgat, J. Cosmol. Astropart. Phys. 10 (2008) 034.

[28] M. Yu. Khlopov, A. G. Mayorov, and E. Yu. Soldatov, Int. J. Mod. Phys. D **19**, 1385 (2010).

[29] M. S. Boucenna and S. Profumo, arXiv:1106.3368.

[30] B. Batell, M. Pospelov, and A. Ritz, Phys. Rev. D **79**, 115019 (2009).

[31] C. Arina, J. Hamann, and Y. Y. Y. Wong, arXiv:1105.5121; M. T. Frandsen *et al.*, arXiv:1105.3734 [Phys. Rev. D (to be published)]; S. Chang *et al.*, J. Cosmol. Astropart. Phys. 08 (2010) 018; M. R. Buckley, D. Hooper, and T. M. P. Tait, arXiv:1011.1499; W. -Y. Keung, I. Low, and G. Shaughnessy, Phys. Rev. D **82**, 115019 (2010).

[32] M. Lisanti and D. N. Spergel, arXiv:1105.4166.

[33] W. Jaffe, Mon. Not. R. Astron. Soc. **202**, 995 (1983).

[34] N. W. Evans, C. M. Carollo, and P. T. de Zeeuw, Mon. Not. R. Astron. Soc. **318**, 1131 (2000).

[35] R. Bernabei *et al.*, Riv. Nuovo Cimento Soc. Ital. Fis. **26N1**, 1 (2003).

[36] R. Bernabei *et al.*, Int. J. Mod. Phys. D **13**, 2127 (2004).

[37] R. Bernabei *et al.*, Nucl. Instrum. Methods Phys. Res., Sect. A **592**, 297 (2008).

[38] R. Bernabei *et al.*, Eur. Phys. J. C **53**, 205 (2008).

[39] R. Bernabei *et al.*, Phys. Lett. B **389**, 757 (1996).

[40] K. Fushimi *et al.*, Phys. Rev. C **47**, R425 (1993).

[41] V. I. Tretyak, Astropart. Phys. **33**, 40 (2010).

[42] H. Chagani *et al.*, arXiv:physics/0611156; E. Simon *et al.*, Nucl. Instrum. Methods Phys. Res., Sect. A **507**, 643 (2003).

[43] S. I. Matyukhin, Tech. Phys. **53**, 1578 (2008).

[44] N. Bozorgnia *et al.*, J. Cosmol. Astropart. Phys. 11 (2010) 19.

[45] D. Hooper and C. Kelso, arXiv:1106.1066.

[46] S. Scopel, S. Choi, N. Fornengo, and A. Bottino, Phys. Rev. D **83**, 095016 (2011).

[47] H. K. Dreiner, S. Heinemeyer, O. Kittel, U. Langenfeld, A. M. Weber, and G. Weiglein, Eur. Phys. J. C **62**, 547 (2009).

[48] A. Bottino, N. Fornengo, G. Polesello, and S. Scopel, Phys. Rev. D **77**, 115026 (2008).

[49] J. A. Conley, H. K. Dreiner, and P. Wienemann, Phys. Rev. D **83**, 055018 (2011).

[50] This value is similar to the one obtained in: D. Hooper and T. Plehn, Phys. Lett. B **562**, 18 (2003); G. Belanger, F. Boudjema, A. Pukhov, and S. Rosier-Lees, arXiv:hep-ph/0212227.

[51] A. Bottino, F. Donato, N. Fornengo, and S. Scopel, Astropart. Phys. **13**, 215 (2000); **18**, 205 (2002).

[52] T. K. Gaisser, G. Steigman, and S. Tilav, Phys. Rev. D **34**, 2206 (1986).

[53] CMS Collaboration, Phys. Lett. B **698**, 196 (2011).

[54] ATLAS Collaboration, Phys. Rev. Lett. **106**, 131802 (2011).
[55] ATLAS Collaboration, Phys. Lett. B **701**, 186 (2011).
[56] V. M. Abazov *et al.* (D0 Collaboration), Phys. Lett. B **660**, 449 (2008).
[57] T. Aaltonen *et al.* (CDF Collaboration), Phys. Rev. Lett. **102**, 121801 (2009).
[58] CMS Collaboration, Phys. Rev. Lett. **106**, 231801 (2011).
[59] CDF Collaboration, D0 Collaboration, and Tevatron New Physics Higgs Working Group (TEVNPHWG), arXiv:1003.3363 (preliminary analysis, unpublished).
[60] J. Baglio and A. Djouadi, arXiv:1103.6247.
[61] C. E. Aalseth *et al.*, Phys. Rev. Lett. **106**, 131301 (2011).
[62] D. T. Cumberbatch *et al.*, arXiv:1107.1604.
[63] P. J. Fox *et al.*, arXiv:1107.0717v1.